IEEE Access
Multidisciplinary | Rapid Review | Open Access Journal

Received March 23, 2019, accepted April 29, 2019, date of publication May 8, 2019, date of current version May 23, 2019.

Digital Object Identifier 10.1109/ACCESS.2019.2915674

Simulation of the Magnetic Signature for Ferromagnetic Objects in Motion Using 3D-Printing Data

YANGYI SUI, (Member, IEEE), KE LIU, (Member, IEEE), SHIBIN LIU, AND ZHENGHUI XIA
Key Laboratory of Geo-exploration Instruments, Ministry of Education of China, Jilin University, Changchun 130026, China
College of Instrumentation and Electrical Engineering, Jilin University, Changchun 130026, China

Corresponding author: Yangyi Sui (suiyangyi@jlu.edu.cn)

This work was supported by the National Natural Science Foundation of China under Grant 41574174.

ABSTRACT Investigations of the magnetic signature for ferromagnetic objects are extremely important in many areas. Some famous software can calculate the magnetic signature generated by the 3D ferromagnetic objects in motion, but they require tremendous computational time and large numerical resources. Therefore, we propose a simulation method whose core idea is to approximate the ferromagnetic object by a collection of magnetic dipoles whose placement is identified with the tool path information generated by 3D printing software and calculate the magnetic signature of the ferromagnetic object using the superposition principle. In view of the fact that each particle of a rigid body has the same laws of motion while the body moving and rotating in 3D space, coordinate translations, and rotations are used to implement the six-degrees-of-freedom movement of ferromagnetic objects. The simulations with a static object and objects in motion in the application of the magnetic test for a satellite validate the correctness of the proposed method. The evaluation of magnetic interference of a survey ship demonstrates the effectiveness. The method is easy to implement and has strong practicability and powerful expansibility.

INDEX TERMS Magnetic instruments, magnetic signature, 3D-Printing, ferromagnetic object, motion.

I. INTRODUCTION

Investigations of the magnetic signature for ferromagnetic objects are of great importance in many areas such as exploring mineral resources [1], tracking moving magnetic targets [2], and degaussing or magnetic compensation for marine vehicle [3]. Simulation of the magnetic signature is a powerful approach in the design of magnetic instruments, verification of data interpretation and support for data presentation. Many famous software such as COMSOL Multiphysics, Ansoft Maxwell and FLUX can be used to calculate the magnetic signature generated by the 3D ferromagnetic objects. They are reliant on the finite element method (FEM) that solves engineering and mathematical physics problems by subdividing a whole domain into smaller parts that are called finite elements, assembling all sets of simple equations that model these finite elements into a global system of equations and obtaining a numerical answer from the initial values of the original problems. While calculating the magnetic signature generated by the 3D ferromagnetic objects in motion, the arbitrary Langrangian-Eulerian (ALE) moving mesh [4], remeshing [5], and significant mesh operations [6] are often required, which consumes tremendous computational time and large numerical resources [4], [7].

In fact, the dielectric properties and magnetic shielding of a moving ferromagnetic object can be negligible when obtaining its magnetic signature around the object, especially in most geophysical applications [8]. Consequently, only the ferromagnetic effects including permanent magnetism and induced magnetism need to be considered, that is ignoring the eddy current magnetism in simulation. In addition, the magnetic signature of a 3D ferromagnetic object could be derived by dividing the object into an array of magnetic dipoles, calculating the magnetic fields and magnetic gradient tensors of each dipole, and then summing the effects of all dipoles [8]. 3D printing creates a physical object from a digital design by adding material together layer by layer and this special process is very similar to the superposition principle summing the effects of all magnetic dipoles.

The associate editor coordinating the review of this manuscript and approving it for publication was Bora Onat.

Therefore, we proposed a simpler and lighter simulation method.

The core idea is to approximate the ferromagnetic object by a collection of magnetic dipoles whose placement is identified with the tool path information generated by 3D printing software and calculate the magnetic signature of the ferromagnetic object using the superposition principle. Note that 3D printing is only used to generate the simulation data rather than the actual object. Furthermore, the six-degrees-of-freedom (6DoF) movement of the ferromagnetic object is implemented by coordinate translations and rotations.

The advantages of the proposed simulation method with 3D-printing data could be summarized as follows:

(1) It is simple and easy to implement. The computational accuracy can be improved regardless of whether the user is a sophisticated expert or not. In contrast, when analyzing a problem with Ansoft Maxwell, the initial mesh is often too coarse for an efficient, accurate field solution and the elaborate mesh operations are often necessary [6].

(2) It has strong practicability. The computational accuracy and the amount of time and memory consumed by the simulation are independent of the mode and complexity of motion. Most simulation software can only consider simple motion like the rotation about one axis or two-degrees-of-freedom movement [9] because various technologies such as the ALE moving mesh are necessary, which takes a tremendous amount of time and memory.

(3) It is perhaps the simplest method to obtain multiple-order magnetic gradient tensors of ferromagnetic objects because of the known analytical tensor expressions of a magnetic dipole. Comparatively speaking, in COMSOL Multiphysics, the differential operators are the key to the calculation of the multiple-order magnetic gradient tensors, therefore an accurate solution relies heavily on the high quality of the mesh element.

(4) The simulation process for multiple ferromagnetic objects in motion or a ferromagnetic object whose parts have various magnetic properties is consistent with that for a single object, so it has powerful expansibility.

II. SIMULATION PROCESS WITH 3D-PRINTING DATA

3D printing, also called additive manufacturing, includes four main types: stereolithography (SLA) [10], selective laser sintering (SLS) [11], laminated object manufacturing (LOM) [12], and fused deposition modeling (FDM) [13]. FDM is widely used by 3D printers nowadays and its general process is [14]:

(1) Build up the model with a computer-aided design (CAD) package or a 3D scanner, and export a stereolithography STL) file, which is an interface in the rapid prototyping system.

(2) Import the STL file into a slicing program cutting the model into layers and produce the machine code that determines the tool path for the machine to follow.

(3) The extrusion nozzle extrudes liquefied plastic filament along the tool path layer by layer until the desired object is completed.

By analogy with the process of the 3D printing, the steps of our proposed simulation method are listed below:

(1) The models of 3D printed objects representing the ferromagnetic objects can be obtained via a CAD package, medicine imaging techniques or a 3D scanner with a suitable scale ratio. Then the 3D models are exported in STL format. With regard to the ferromagnetic object whose parts have various magnetic properties, output the corresponding STL files for each part respectively.

(2) Import each STL file into Slic3r, which is a 3D slicing engine for 3D printers. Slic3r converts the model into a series of thin layers, and then produces a G-code file (a numerical control programming language used in computer-aided manufacturing). The *print*, *filament* and *printer settings* need to be altered in Slic3r to get accurate placement information of the simulated objects. Then set the *layer height*to the default value for the first time and keep the *extrusion width* equal to the *layer height*. Finally, obtain a 3D printed object with no void space by setting the fill pattern to *rectilinear* and the fill density to 100% to represent the completely filled in object in the real world effectively.

(3) The G-code file encompasses the instructions that tell the motors where to move, how fast to move, and what path to follow. The primary commands in the G-code file are the G-commands that tell the control what kind of motion is wanted or what offset value to use and the E-commands that control the length of extrudate. For example, the G-code file from Slic3r includes G1-commands (Linear Move) which indicate the starting and ending points on the tool path, E-commands which tell the amount of extrudate between the starting and ending points and parameters which tell the positions to move to on the x, y, and z axis. Parse the G-code file to gain the coordinates of the starting and ending points on the tool path and the information whether the material is extruded from the nozzle or not. If the answer is yes, simulate the extrusion process of the nozzle by interpolating intermediate points between the starting and ending points, and the interpolation interval is set in accordance with the *layer height*; otherwise the interpolation is cancelled. The starting, ending and interpolation points are all called as the printing points representing the uniform discrete points in the 3D printed object. Thus, the coordinates of all points in the actual ferromagnetic object are the product of those of printing points in the 3D printed object and the scale ratio.

(4) The ferromagnetic object can be approximated by a collection of magnetic dipoles whose distribution and magnetic moments are set according to the data obtained from the G-code file. Specifically, set each printing point as a magnetic dipole and its dipole

moment $\boldsymbol{m}$ is given by the product of its magnetization $\boldsymbol{M}$ and its volume dv, that is, $\boldsymbol{m} = \boldsymbol{M}$•d$v$. For the induced magnetism, the direction of $\boldsymbol{M}$ is set in the direction of the background magnetic field and its magnitude is given by the relative permeability μ_r of the material and the magnetic field intensity of the background magnetic field. For the permanent magnetism, the direction and magnitude of $\boldsymbol{M}$ are given directly according to its magnetic properties. For example, the values of relative permeability ($\mu_r = 3.5$) and permanent magnetization ($M = 60$ A/m) are commonly used in simulations of magnetic prospecting of iron ore deposits [15]. In general, ferromagnetic objects are normally assumed to be uniformly magnetized in the geomagnetic field [8]. Hence M can be assumed as a constant for each part of the object.

(5) In view of the fact that each particle of a rigid body has the same laws of motion while the body moving and rotating in three-dimensional space, coordinate translations and rotations can be used to implement the 6DoF movement of ferromagnetic objects. The magnetic signature generated by the ferromagnetic objects in motion is derived by calculating the magnetic fields and magnetic gradient tensors of each magnetic dipole and summing the effects of all dipoles. The magnetic field and the components of magnetic gradient tensor of a magnetic dipole are expressed by (1) and (2)

$$\boldsymbol{B} = \frac{\mu_0}{4\pi} \cdot \frac{m}{r^3} \left[3\left(\hat{\boldsymbol{m}} \bullet \hat{\boldsymbol{r}}\right)\hat{\boldsymbol{r}} - \hat{\boldsymbol{m}}\right] \tag{1}$$

$$G_{ij} = -3\frac{\mu_0}{4\pi} \frac{(\boldsymbol{m} \bullet \boldsymbol{r})\left(5r_i r_j - r^2\delta_{ij}\right) - r^2\left(r_i m_j + r_j m_i\right)}{r^7} \tag{2}$$

where $\boldsymbol{m} = m\hat{\boldsymbol{m}}$ is the dipole moment, $\boldsymbol{r} = r\hat{\boldsymbol{r}}$ is the source-to-sensor bearing vector, μ_0 is the permeability of the air, δ_{ij} is the Kronecker's delta, and $i, j = 1, 2$, and 3 represent x, y, and z in the Cartesian coordinate system.

(6) Return to the second step and reset the *layer height* to half of the previous value. Rerun step (2) – (5) and calculate the relative error between the current and previous values of the magnetic signature at the observation point. Repeat these steps until the relative error falls below a tolerance.

(7) For multiple ferromagnetic objects, return to the first step; for the object whose parts have various magnetic properties, return to the second step or use multiple extruders with the similar method.

The comparison between the proposed simulation method with 3D-printing data and FDM is shown in Fig. 1.

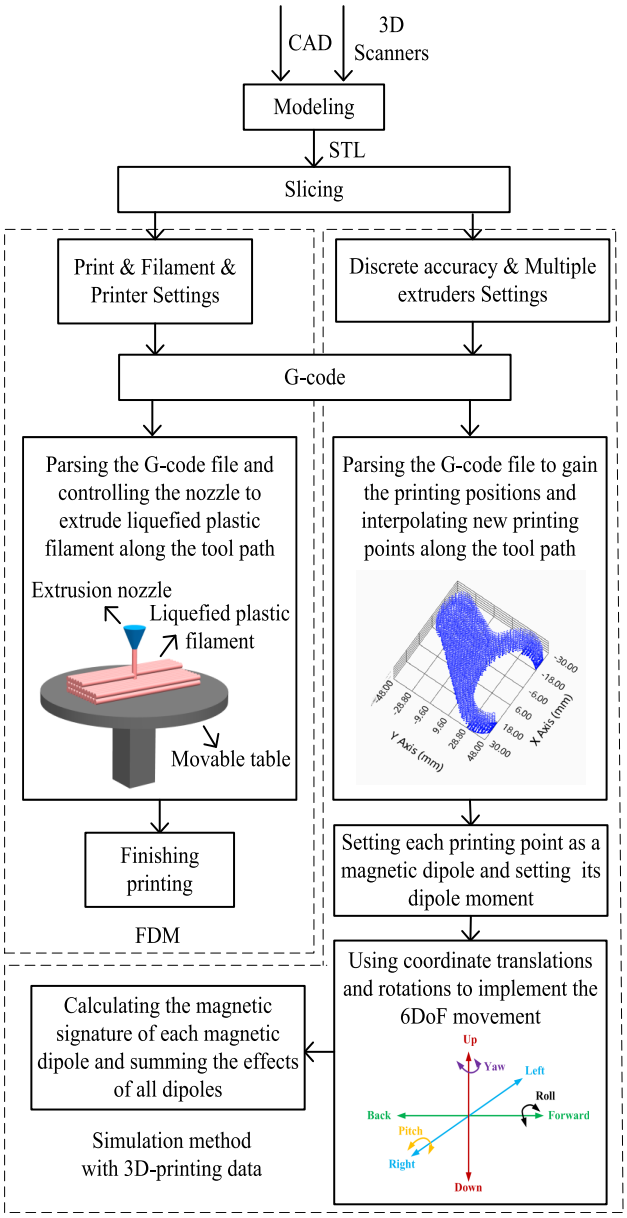

FIGURE 1. Comparison between the proposed simulation method with 3D-printing data and FDM.

III. TEST OF THE SIMULATION METHOD

A. TEST BY A STATIC OBJECT

In order to prove the correctness of the proposed method for a static 3D object, we compare the magnetic signature for a static thin sheet obtained by our method and the FEM method in COMSOL Multiphysics and apply the tensor Euler deconvolution to the sheet with the magnetic fields and gradient tensors calculated by our method.

The thin sheet dimensions are 25 mm radius, 5 mm thickness, and the permanent magnetization of the shin sheet is 0.5 A/m. The *layer height*is set to the default value (0.3 mm) and the *extrusion width*and interpolation interval are equal to the *layer height*. There are 475514 magnetic dipoles used in the thin sheet and their coordinates are obtained by parsing the G-code file and interpolation, shown in Fig. 2. We simulate the three components of the magnetic fields on the line 10 mm above the center of the sheet, and the comparisons between the results obtained by our method and COMSOL are illustrated in Fig. 3. The results demonstrate that our method is correct and feasible.

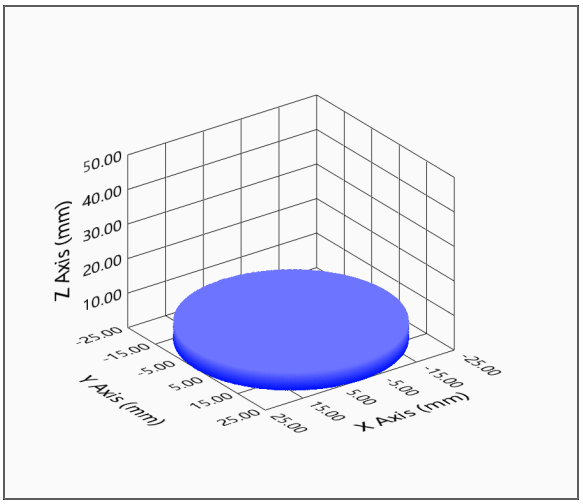

FIGURE 2. Coordinates of all printing points of the thin sheet obtained by parsing the G-code file and interpolation.

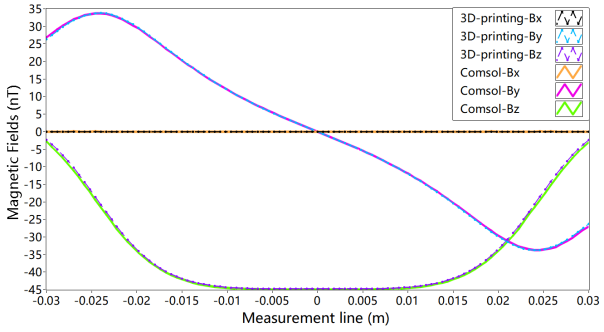

FIGURE 3. Three components of the magnetic fields for the thin sheet on the measurement line simulated by 3D-printing method and the FEM method in COMSOL multiphysics. Comparisons show the correctness of our method.

Tensor Euler deconvolution is a method to determine depths and locations of a magnetic object using the full components of magnetic gradient tensor and magnetic field [16]. It includes three equations

$$(x - x_0) B_{xx} + (y - y_0) B_{xy} + (z - z_0) B_{xz} = N (b_x - B_x) \tag{3}$$

$$(x - x_0) B_{yx} + (y - y_0) B_{yy} + (z - z_0) B_{yz} = N \left(b_y - B_y\right) \tag{4}$$

$$(x - x_0) B_{zx} + (y - y_0) B_{zy} + (z - z_0) B_{zz} = N (b_z - B_z) \tag{5}$$

where x_0, y_0, and z_0 are the unknown coordinates of the magnetic object center or edge, and x, y, and z are the known coordinates of the observation points. B_x, B_y, and B_z are three components of magnetic field; B_{xx}, B_{xy}, B_{xz}, B_{yx}, B_{yy}, B_{yz}, B_{zx}, B_{zy} and B_{zz} are nine components of magnetic gradient tensor; b_x, b_y, and b_z are the regional values of the magnetic field to be estimated and N is the structural index. Thus, n observation points have $3n$ equations containing six unknowns. When $n > 2$, we can solve for the source position and the regional values (x_0, y_0, z_0, b_x, b_y, and b_z).

The measurement area (100 mm × 100 mm) is 10 mm above the top of the thin sheet. Window size of 5 × 5 (25 mm × 25 mm) was used on the grids and the window was moved with a step size twice the grid cell side (5 mm). The structural index of 2.0 was found to outline the edge of the object clearly.

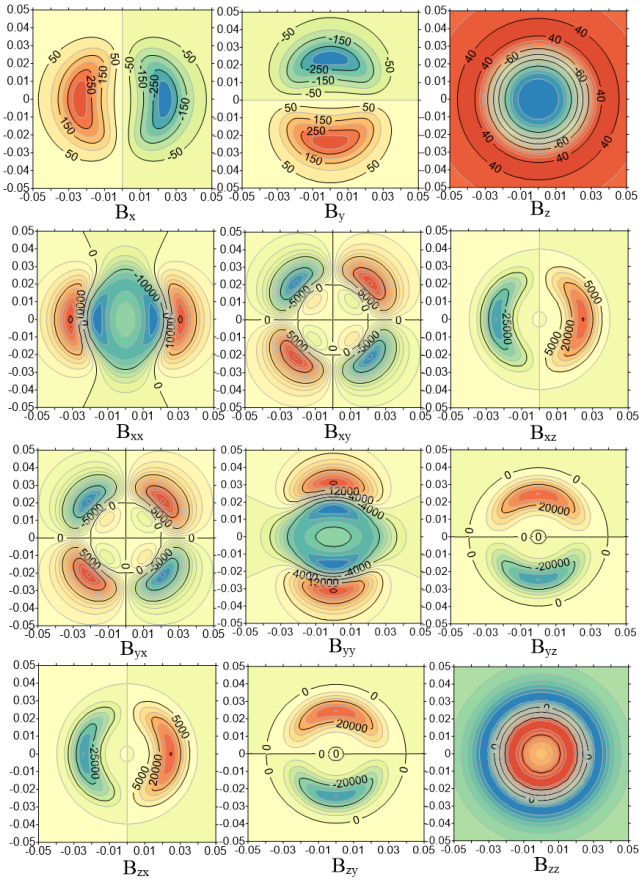

FIGURE 4. Plots of the magnetic fields and the nine components of the magnetic gradient tensors for the thin sheet on the measurement area.

Plots of the magnetic fields and the nine components of the magnetic gradient tensors for the thin sheet on the measurement area are shown in Fig. 4 and the tensor Euler deconvolution results are plotted in Fig. 5. The results also demonstrate that our method is correct and feasible.

B. TEST BY OBJECTS IN MOTION

In order to prove the correctness and effectiveness of the proposed simulation method for ferromagnetic objects in motion, we chose the application of the magnetic test for a satellite.

It is extremely important to know the magnetic fields generated by some ferromagnetic components in a scientific satellite, which provides a basis for magnetic cleanliness design [17]. It is a practical and proven method in magnetic test that rotating the satellite about the vertical axis and the horizontal axis of a swivel table respectively [18], [19].

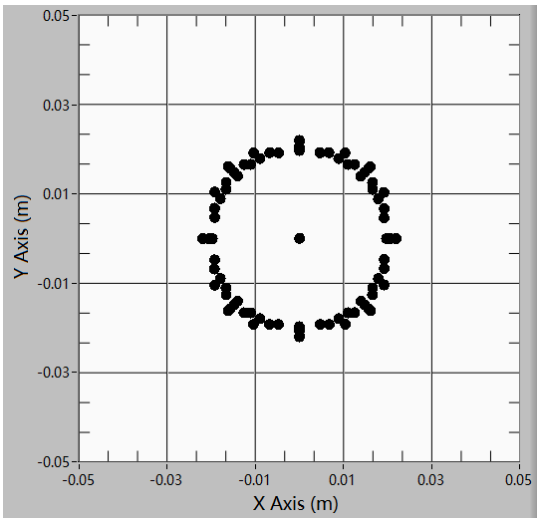

FIGURE 5. Tensor euler deconvolution results of the thin sheet with a dot representing each estimated position.

Therefore, we rotated three magnetorquers and three momentum wheels which are the representatives of soft and hard magnetic materials respectively, and have been widely utilized in attitude control of satellites [20]–[22].

The simulated satellite is a 200 mm × 200 mm × 200 mm cube. The magnetic momentum wheel with the diameter of 75 mm and the height of 7.5 mm has the axial permanent magnetic moment of 1.3 A•m^2 [23]. The magnetorquer with the size of Φ 15 mm × 150 mm has the equivalent induced magnetic moment of 0.5 A•m^2 [24] due to uniformly magnetized by the ambient magnetic field along z axis. The numbers of magnetic dipoles used in the magnetic momentum wheel and the magnetorquer are 221984 and 231317 respectively. According to the design of attitude control systems for a CubeSat researched by the scholars at York University, Canada [25], we set three momentum wheels and three magnetorquers on the x, y and z axis, respectively, shown in Fig. 6. Set the observation point on the x axis with 500 mm distance from the satellite center and the simulation results are illustrated in Fig. 7.

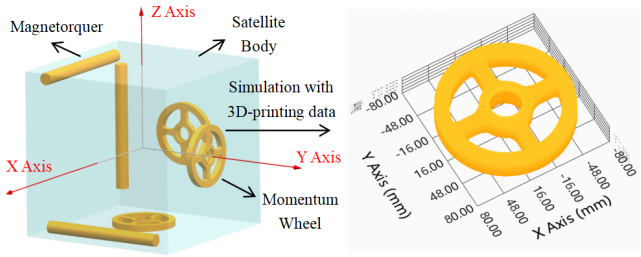

FIGURE 6. Three magnetorquers and three momentum wheels are placed in the satellite for attitude control.

According to the results obtained above, we determined the equivalent magnetic dipole moment of the satellite by the field analysis [19]. The method derives the equations of the

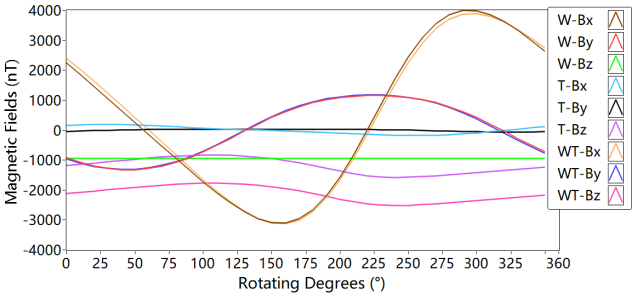

FIGURE 7. Three components of magnetic fields produced by magnetorquers (T), momentum wheels (W) and their superposition (WT), respectively.

magnetic fields at three observation points from the rotating satellite and solves the magnetic dipole moment by the least squares method. When an observation point is far from the satellite, it can be approximately equivalent to a magnetic dipole and its equivalent magnetic moment $\boldsymbol{m}_e$ is equal to the moment sum of the six components of the satellite. The magnetic dipole moment $\boldsymbol{m}_c$ calculated by the field analysis also denotes the sum of induced and permanent moments. The equivalent and calculated magnitude of magnetic moments corresponding to the different locations of observation points are illustrated in Table 1.

TABLE 1. Magnitude of magnetic moments.

Observation points (m)			Calculated moment m_{cx} / m_{cy} / m_{cz} / $\|m_c\|$ (A•m^2)	Equivalent moment m_{ex} / m_{ey} / m_{ez} / $\|m_e\|$ (A•m^2)	Error of $\|m\|$ (A•m^2)
0.2	0.3	0.4	1.9501/2.3976/ 1.7066/3.5304	1.3000/1.3000 /2.8000/3.349 6	0.1808
0.4	0.5	0.6	1.4073/1.5486/ 2.5954/3.3338		0.0158
0.6	0.7	0.8	1.3446/1.4077/ 2.7147/3.3405		0.0091
0.8	0.9	1.0	1.3248/1.3605/ 2.7526/3.3441		0.0055
1.8	1.9	2.0	1.3050/1.3124/ 2.7904/3.3484		0.0012

Table 1 shows that the farther the observation point is from the satellite, the more exactly the ferromagnetic objects can be equivalent to a magnetic dipole, as expected, which demonstrates that the proposed simulation method with 3D-printing data is correct and feasible for 3D ferromagnetic objects in motion.

IV. APPLICATION IN MARINE MAGNETIC SURVEY

Marine magnetic survey is a groundwork for archaeology, exploring mineral and petroleum resources, locating seabed ferromagnetic objects, and building the World Digital Magnetic Anomaly Map etc. [26], [27]. Survey ships are sources of magnetic interference on magnetometers, because they

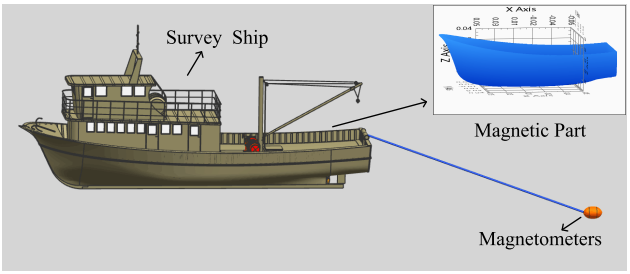

FIGURE 8. Schematic of a marine magnetic survey. Magnetometers are dragged far from the ship to reduce the effects of magnetic interference.

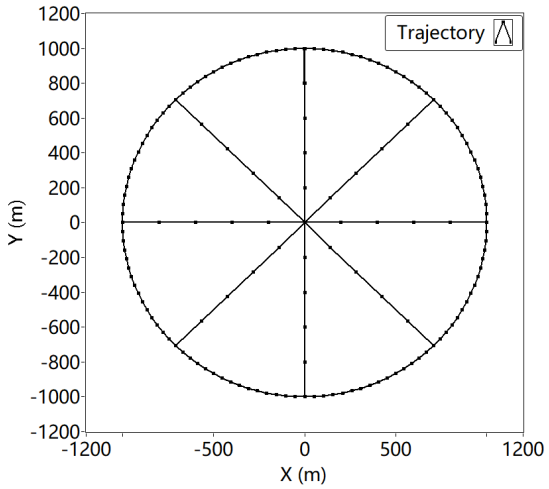

FIGURE 9. The trajectory of the ship during the survey for standard magnetic compensation.

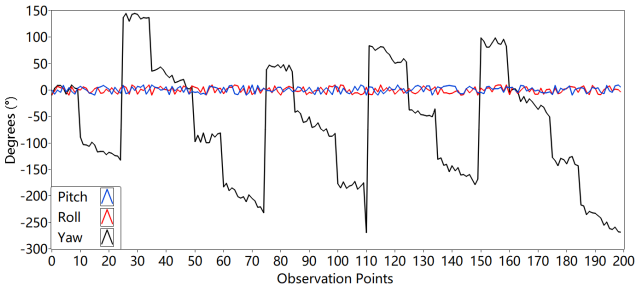

FIGURE 10. The attitude of the ship with an additive fluctuation in the range of −10° to 10° during the survey.

are mostly made of ferromagnetic materials and magnetized inevitably by the omnipresent earth's magnetic field. Therefore, the evaluation and elimination of the effect of magnetic interference are vital for the data quality of magnetic instruments. The widely used equivalent magnetic models are the magnetic dipole model and the ellipsoid model, but their applicable conditions are both limited [28].

The 6DoF movement of the survey ship and the magnetometers are both dynamically changed during a marine survey, which is extremely suitable for demonstrating the advantages of our proposed method. In addition, the multiple-order magnetic gradient tensors can be obtained easily because of the known analytical tensor expressions of a magnetic dipole, which is meaningful for modern instruments measuring the full magnetic gradient tensor in the earth's magnetic field [29].

Since the survey ship has been artificially demagnetized many times before being put into use, the permanent magnetism of the survey ship can be negligible, and the induced magnetism has a major impact on magnetometers [30]. In this simulation, we considered the main hull of the survey ship which only has induced magnetism with the length of 20 m, the width of 7 m and the height of 4 m (the 3D printed ship was modeled with the scale ratio of 100 smaller than the actual survey ship), and the magnetometers towed 50 m astern of the ship. The number of magnetic dipoles used in the survey ship is 1152517. Schematic of a marine magnetic survey is shown in Fig. 8.

Let the magnetization magnitude of the survey ship be 0.0165 A/m [9], magnetization declination and inclination be −9° and 60° respectively. The survey ship was controlled to sail along the path of eight directions for standard magnetic compensation, shown in Fig. 9. Three attitude angles (pitch, yaw, and roll) added a random fluctuation in the range of −10° to 10° for both the ship and the magnetometers, shown in Fig. 10. We used coordinate translations and rotations to simulate the 6DoF movement of the survey ship and the magnetometers, and obtained the magnetic fields and the second-order magnetic gradient tensors that should be measured by the magnetometers in the actual survey. The results

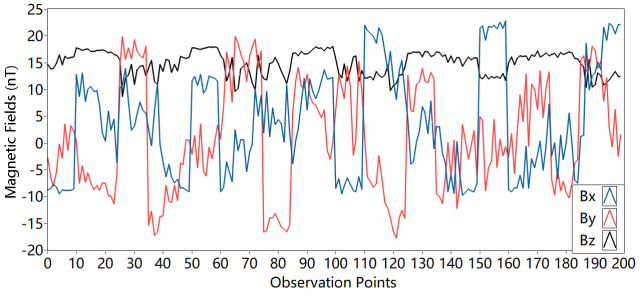

FIGURE 11. Three components of magnetic fields produced by the 6DoF movement of the survey ship.

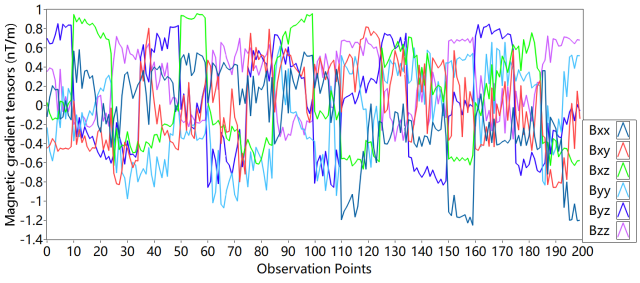

FIGURE 12. Six components of second-order magnetic gradient tensors produced by the 6DoF movement of the survey ship.

of the magnetic fields and gradient tensors are illustrated in Fig. 11 and Fig. 12 respectively.

In contrast, Birsan etc. have used an earth's magnetic field simulator with the finite element geometrical structure fixed and sine signals regularly varied with time to simulate the effect of roll and pitch motion on ship magnetic signature [9]. Obviously, only two-degrees-of-freedom movement can be simulated and the mode of two motion is limited.

V. CONCLUSION

The proposed simulation method can be applied in many fields such as a magnetic test for a scientific spacecraft, preliminary work for inversion in magnetic survey, and analysis of interference on high-precision magnetic instruments. More complex functions can also be achieved by setting the magnetic property of dipoles as a function of time, temperature or other physical parameters. The proposed method has many merits for 3D ferromagnetic objects in complex motion because the mesh division in the computational domain far from the ferromagnetic objects is not required, which is indispensable in other simulation software and results in lower accuracy, tremendous computational time and large numerical resources. In addition, it has one advantage than common commercial or open-source software for static 3D objects, that is to obtain accurate multiple-order magnetic gradient tensors easily. However, the method can only be used to obtain the magnetic signature outside a ferromagnetic object.

REFERENCES

[1] R. S. Smith, A. Salem, and J. Lemieux, "An enhanced method for source parameter imaging of magnetic data collected for mineral exploration," *Geophys. Prospecting*, vol. 53, no. 5, pp. 655–665, 2005.
[2] L. Fan *et al.*, "Tracking of moving magnetic target based on magnetic gradient system with total field magnetometers," *Sensor Rev.*, vol. 38, no. 4, pp. 501–508, Sep. 2018.
[3] J. J. Holmes, "Reduction of a ship's magnetic field signatures," *Synth. Lect. Comput. Electromagn.*, vol. 3, no. 1, pp. 1–68, Jan. 2008.
[4] W. Choi, S. H. Lee, C.-T. Kim, and S. Jun, "A finite element method based flow and heat transfer model of continuous flow microwave and ohmic combination heating for particulate foods," *J. Food Eng.*, vol. 149, pp. 159–170, Mar. 2015.
[5] *COMSOL Multiphysics Reference Manual, Version 5.3*, COMSOL AB, Stockholm, Sweden, 2017, p. 1480.
[6] *ANSYS Maxwell V16 Training Manual Lecture 6: Meshing and Mesh Operations*, ANSYS, Canonsburg, PA, USA, 2013.
[7] M. Dal, P. Le Masson, and M. Carin, "A model comparison to predict heat transfer during spot GTA welding," *Int. J. Therm. Sci.*, vol. 75, no. 16, pp. 54–64, 2014.
[8] R. J. Blakely, *Potential Theory in Gravity and Magnetic Applications*. Cambridge, U.K.: Cambridge Univ. Press, 1995.
[9] M. Birsan and R. Tan, "The effect of roll and pitch motion on ship magnetic signature," *J. Magn.*, vol. 21, no. 4, pp. 503–508, 2016.
[10] C. W. Hull, "Apparatus for production of three dimensional objects by stereolithography," U.S. Patent 6 027 324, Feb. 22, 2000.
[11] P. K. Venuvinod and W. Ma, "Selective laser sintering (SLS)," in *Rapid Prototyping*. Boston, MA, USA: Springer, 2004, pp. 245–277.
[12] J. Park, M. J. Tari, and H. T. Hahn, "Characterization of the laminated object manufacturing (LOM) process," *Rapid Prototyping J.*, vol. 6, no. 1, pp. 36–50, Mar. 2000.
[13] C. K. Chua, K. F. Leong, and C. S. Lim, *Rapid Prototyping: Principles and Applications*. Singapore: World Scientific, 2003.
[14] *Design Guide: Fused Deposition Modeling (FDM)*, Xometry, Gaithersburg, MD, USA, 2016.
[15] G. Kletetschka, P. J. Wasilewski, and P. T. Taylor, "Hematite vs. Magnetite as the signature for planetary magnetic anomalies," *Phys. Earth Planet. Interiors*, vol. 119, pp. 259–267, May 2000.
[16] C. Zhang, M. F. Mushayandebvu, A. B. Reid, J. D. Fairhead, and M. E. Odegard, "Euler deconvolution of gravity tensor gradient data," *Geophysics*, vol. 65, no. 2, pp. 512–520, 2000.
[17] P. W. Droll and E. J. Jufer, "Magnetic properties of selected spacecraft materials," Symp. Space Magi. Nic Explor. Technol., USA, Eng. Rep. 9, 1967, pp. 189–197.
[18] R. Moskowitz and R. Lynch, "Magnetostatic measurement of spacecraft magnetic dipole moment," *IEEE Trans. Aerosp.*, vol. 2, no. 2, pp. 412–419, Apr. 1964.
[19] W. L. Eichhorn, "Magnetic dipole moment determination by near-field analysis," NASA Goddard Space Flight Center, Greenbelt, MD, USA, Tech. Rep. TN D-6685, 1972.
[20] F. Yin, H. Lühr, J. Rauberg, I. Michaelis, and H. Cai, "Characterization of CHAMP magnetic data anomalies: Magnetic contamination and measurement timing," *Meas. Sci. Technol.*, vol. 24, no. 7, 2013, Art. no. 075005.
[21] T. Inamori, K. Otsuki, Y. Sugawara, P. Saisutjarit, and S. Nakasuka, "Three-axis attitude control by two-step rotations using only magnetic torquers in a low Earth orbit near the magnetic equator," *Acta Astronautica*, vol. 128, pp. 696–706, Nov./Dec. 2016.
[22] K. Sathyan, H. Y. Hsu, S. H. Lee, and K. Gopinath, "Long-term lubrication of momentum wheels used in spacecrafts—An overview," *Tribol. Int.*, vol. 43, nos. 1–2, pp. 259–267, 2010.
[23] L. Yun, F. Jiancheng, and T. Jiqiang, "Research on analysis and compensation method of remnant magnetic moment for magnetically suspended reaction flywheel," *Acta Aeronautica Astronatica Sinica*, vol. 32, no. 5, pp. 881–890, 2011.
[24] N. Sugimura, T. Kuwahara, and K. Yoshida, "Attitude determination and control system for nadir pointing using magnetorquer and magnetometer," in *Proc. IEEE Aerosp. Conf.*, Mar. 2016, pp. 1–12.
[25] J. Li, M. Post, T. Wright, and R. Lee, "Design of attitude control systems for CubeSat-class nanosatellite," *J. Control Sci. Eng.*, vol. 2013, Jan. 2013, Art. no. 4.
[26] D. Hrvoic, "High-resolution near-shore geophysical survey using an autonomous underwater vehicle (AUV) with integrated magnetometer and side-scan sonar," Ph.D. dissertation, McMaster Univ., Hamilton, ON, Canada, 2014.
[27] Y. Quesnel, M. Catalán, and T. Ishihara, "A new global marine magnetic anomaly data set," *J. Geophys. Res., Solid Earth*, vol. 114, no. 4, pp. 1–11, 2009.
[28] G. Shengfeng, Z. Hai, W. Chao, and C. Peng, "Analysis on the applicability of submarine magnetic model based on finite-element method," *Ship Sci. Technol.*, vol. 38, no. 1, pp. 34–38, 2016.
[29] S. T. Keenan, D. Clark, K. R. Blay, K. Leslie, C. P. Foley, and S. Billings, "Calibration and testing of a HTS tensor gradiometer for underwater UXO detection," in *Proc. Int. Conf. Appl. Supercond. Electromagn. Devices (ASEMD)*, 2011, pp. 135–137.
[30] A. V. Kildishev and J. A. Nyenhuis, "External magnetic characterization of marine vehicles," in *Proc. MTS/IEEE Conf. Exhib.*, Sep. 2000, pp. 1145–1147.

YANGYI SUI (M'18) received the B.Eng., M.S., and Ph.D. degrees from Jilin University, Changchun, China, in 2002, 2005, and 2008, respectively.

He is currently a Professor with the College of Instrumentation and Electrical Engineering, Jilin University. His current research interests include magnetic measurement, and magnetic gradient tensor measurement systems and their applications, especially based on unmanned platforms.

KE LIU (M'18) received the B.Eng. degree in electrical engineering and automation from North China Electric Power University, Beijing, China, in 2017. She is currently pursuing the Ph.D. degree in measurement technology and instruments with Jilin University, Changchun, China.

Her current research interests include magnetic gradient tensor measurement systems and their application, and data quality assessment of aeromagnetic data.

SHIBIN LIU received the B.Eng. degree in electrical engineering and automation from Jilin University, Changchun, China, in 2016, where he is currently pursuing the Ph.D. degree in detection technology and automatic equipment.

His current research interests include the calibration of magnetic gradient tensor measurement systems and the inversion from magnetic gradient tensor data.

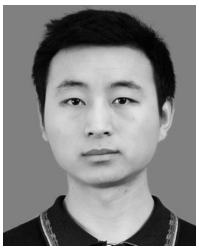

ZHENGHUI XIA received the B.Eng. degree from Jilin University, Changchun, China, in 2016, where he is currently pursuing the M.S. degree in electrical engineering and automation.

His main research interest includes the development of magnetic tensor gradient systems based on rotation modulation.